The 2009 IEEE/RSJ International Conference on
Intelligent Robots and Systems
October 11-15, 2009 St. Louis, USA

Illumination Position Estimation for 3D Soft-Tissue Reconstruction in Robotic Minimally Invasive Surgery

Danail Stoyanov, Dan Elson and Guang-Zhong Yang

Abstract— **For robotic assisted minimally invasive surgery, recovering the 3D soft-tissue shape and morphology *in vivo* is important for providing image-guidance, motion compensation and applying dynamic active constraints. In this paper, we propose a practical method for calibrating the illumination source position in monocular and stereoscopic laparoscopes. The method relies on using the geometric constraints from specular reflections obtained during the laparoscope camera calibration process. By estimating the light source position, the method forgoes the common assumption of coincidence with the camera centre and can be used to obtain constraints on the normal of the surface geometry during surgery from specularities. We demonstrate the effectiveness of the proposed approach with numerical simulations and by qualitative analysis of real stereo-laparoscopic calibrations.**

I. Introduction

The introduction of surgical robots in minimally invasive surgery (MIS) has enabled enhanced surgical dexterity through the use of articulated mechanical wrists controlled via microprocessors. By providing motion scaling and tremor cancellation, such systems can be used to perform micro-scale tasks that are not possible using traditional laparoscopic instruments [1]. However, there are still several significant challenges in robotic assisted MIS that arise due to the limited and distal access to the internal anatomy coupled with soft-tissue deformation. In these cases, integration of pre-operative and intra-operative data is a major difficulty [2]. For advanced surgical robotics, determining the 3D surface shape and motion of the soft-tissue during surgery is important for providing the surgeon with intra-operative guidance, motion stabilization, and applying image-guided active constraints to enhance the surgeon's capabilities in the dynamic and confined workspace [3].

Early work on recovering the 3D surface of the soft-tissue in MIS is mainly focused on monocular techniques, particularly, the use of shape-from-shading (SfS) [4,5,6]. A common assumption used in SfS methods is that the illumination source is located at the camera centre [4] and while modern SfS techniques used in MIS have been extended to handle more complex projection models [7] the illumination condition has remained. This simplifies the SfS equations and makes the problem more easily tractable. However, the coincidence of the camera centre and the light source is only an approximation and can vary considerably between different scopes. The diameter of devices used in MIS is around 11mm and the distance between the incoherent fibre bundle channeling light to the surgical site and the camera is inherently small. This is not insignificant, however, because the distance between the observed tissue's geometry and the imaging device is also small, typically ranging between 40mm and 100mm. In addition, an increasing number of scopes include several illumination channels as shown in Fig 1 and this setup is common with stereo-laparoscopes as used in robotic surgery systems like the daVinci. There is also a recent trend for introducing multiple illumination sources for enhancing surgical guidance [8] and it is therefore desirable to devise an explicit technique for estimating illumination positions.

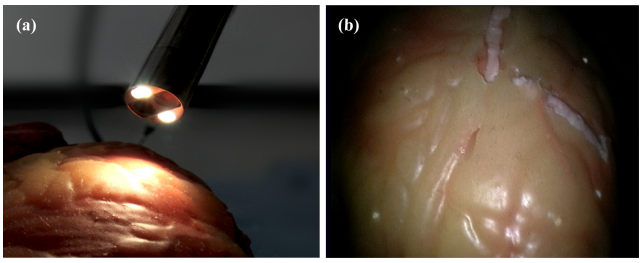

Fig. 1. (a) Stereo-laparoscope of the daVinci surgical system showing two illumination sources and two cameras observing a silicone phantom model; (b) image from one camera of the scope in (a) illustrating the presence of specular highlights that can provide information about the observed surface shape.

In addition to SfS methods, with the introduction of stereo-laparoscopes notable progress has been made for recovering metric 3D measurements of the *in vivo* morphology and structure of soft-tissues [9,10,11]. In order to track tissue deformation over time, these methods assume a geometric surface model in the form of free-form bilinear grids or thin-plate splines [10,11]. The geometric model is recalculated at each time interval subject to optimizing an image similarity measurement, which can be adversely affected by view dependent specular reflections. In order to avoid errors caused by specularities the highlights are usually detected and subsequently removed or interpolated to ignore their interference [11,12,13]. While this approach is computationally efficient, it discards the valuable information specular reflections convey about the imaging geometry and the surface shape.

Manuscript received March 8, 2009 and revised July 30, 2009. This work was supported in part by the EPSRC/TSB funded Robotic Assisted Surgical Guidance and Visualisation (DT/E011101/1) and the EC FP7 funded ARAKNES (224565).

D. Stoyanov, D. Elson and G.-Z. Yang are with the Institute of Biomedical Engineering and the Department of Biosurgery and Surgical Technology, Imperial College London, SW7 2AZ, UK (phone: +44-207-5940805; fax: +44-207-5940805; e-mail: danail.stoyanov@ imperial.ac.uk).

In practice, specular reflections can be used to estimate surface shape and to constrain metric 3D reconstruction [14,15]. Given the rigidly fixed relationship between the camera and illumination source in MIS visualization devices, it is possible to use specular reflections to obtain important information regarding the soft-tissue surface normal. This can be utilized both for shading information and for improving stereo techniques. To determine the surface orientation and use this constraint in shape estimation for MIS it is important to know the illumination position.

In this study, we have developed a method for estimating the light source position in MIS by using the specular reflections caused by the light source during preoperative camera calibration. The method only requires the customary planar calibration object used for laparoscope calibration to be reflective. Specular highlights detected in the image are then used to triangulate the illumination position with respect to the camera. The method is efficient and practical to implement and can be seamlessly deployed in practical MIS.

II. Background

A. Camera Geometry

We express the relationship between image and world coordinates using the pinhole camera model [16]. This uses the internal parameters of the camera and its orientation in the scene to project 3D points onto the image plane. The projection can be effectively described by matrix multiplication using homogeneous notation and the mapping between a world point $\mathbf{M} = [X \quad Y \quad Z \quad 1]^{\mathsf{T}}$ and an image point $\mathbf{m} = [x \quad y \quad 1]^{\mathsf{T}}$ can be represented by the following equation:

$$\mu\mathbf{m} = \mathbf{K}\big[\mathbf{R} \mid \mathbf{t}\big]\mathbf{M} = \mathbf{P}\mathbf{M} \tag{1}$$

where μ is a scale factor and $\mathbf{P}$ is the projection matrix, combining the intrinsic parameter matrix $\mathbf{K}$ and the extrinsic orientation parameters $\mathbf{R}$ and $\mathbf{t}$. For stereo-laparoscopes each camera is modeled independently but one is selected as the reference world coordinate system. Imaging systems in MIS typically require non-linear lens distortion modeling and compensation and in this study we assume the distortion parameters are determined during calibration and images are warped for radial and tangential distortion correction.

For a calibrated laparoscope camera, a ray $\mathbf{q}(\mathbf{m})$ defining the line of sight for an image point $\mathbf{m}$ can be derived by using the camera matrix and the optical centre of the camera as:

$$\mathbf{q}\big(\mathbf{m}\big) = \mathbf{c} + \lambda\mathbf{P}^{\dagger}\mathbf{m} \tag{2}$$

where $\mathbf{c}$ denotes the optical centre and $\mathbf{P}^{\dagger}$ the Moore-Penrose pseudo inverse of the projection matrix. The parameter λ represents the depth along the direction of $\mathbf{q}(\mathbf{m})$ and we assume that all line of sight rays are normalized such that $\big\|\mathbf{q}(\mathbf{m})\big\| = 1$. In the case of stereo imaging, when the calibration parameters are known, the 3D position of a landmark visible from both stereo-laparoscope views can be computed by finding the intersection of the rays back-projected from each camera.

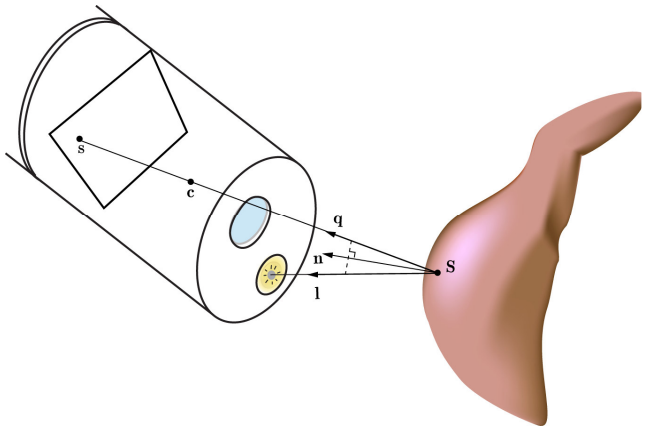

Fig. 2. The specular reflection geometry showing the soft-tissue surface normal bisecting the angle between the viewing direction and the illumination direction.

B. Specular Reflection Geometry

The condition for specular reflection is that the surface normal $\mathbf{n}$ at the 3D point $\mathbf{S}$ where the specularity occurs, bisects the direction of incident light $\mathbf{l}$ and the viewing direction defined by the light of sight. This means that for any given specular point $\mathbf{s}$ in the image, the corresponding line of sight ray $\mathbf{q}(\mathbf{s})$ and the surface normal provide a constraint on the direction of the light source. This relationship is shown in Fig 2 and can be expressed as the following constraint:

$$\mathbf{n} = \frac{\mathbf{l} - \mathbf{q}(\mathbf{s})}{\big\|\mathbf{l} - \mathbf{q}(\mathbf{s})\big\|} \tag{3}$$

In the general case of a calibrated camera, only the direction ray $\mathbf{q}(\mathbf{s})$ may be calculated from a detected specularity. The surface normal and illumination directions are unknown and it should also be noted that the depth of the point $\mathbf{S}$ along $\mathbf{q}(\mathbf{s})$ where the reflection occurs is also unknown.

III. Calibration Procedure

For calibrating the surgical camera, it is typical to use an offline procedure before the imaging device is inserted into the patient. The calibration method based on homographies [13] is usually adapted for this task using a planar calibration target. During this process the external orientation of the calibration target is computed for each discrete observation used in the parameter computation. In additional to the traditional approach, we assume that the calibration target is

made of a reflective material, which is not diffuse and exhibits specular reflection. By detecting the specularities at each target orientation we build up constraint in order to estimate the illumination position. In the following, sections we describe the process for monocular and stereoscopic devices.

A. Monocular Case

The orientation of the calibration plane is known at each viewpoint from the calibration information. Hence, we can calculate the equation of the plane in the form $aX + bY + cZ = d$ where the normal of the plane is $\mathbf{n} = [a \quad b \quad c]^{\mathrm{T}}$ and it is normalized such that $\|\mathbf{n}\| = 1$. Because we can calculate the intersection of the plane with a specular ray $\mathbf{q}(\mathbf{s})$ computed from the image we can obtain the 3D position of the specular point $\mathbf{S}$ on the calibration target. From (3), at this position, the direction of the light source must satisfy the following equation:

$$\mathbf{l} = \mathbf{q}(\mathbf{s}) - 2(\mathbf{n} \cdot \mathbf{q}(\mathbf{s}))\mathbf{n} \tag{4}$$

At each orientation of the calibration target the observation of specular highlights provides a constraint on the position of the light source $\mathbf{L}$. By obtaining more than one view of the calibration plane is possible to triangulate the light source position by finding the intersection of collected illumination directions $\mathbf{l}_i$. This concept is illustrated in Fig 3 where the calibration object has been moved to obtain different views. One should not that moving the scope and keeping the calibration target fixed results in the same constraints.

In practice, the estimated directions of the light source $\mathbf{l}_i$ will not intersect at the same single point. This is the result of noise and imprecision in the image measurements of specular reflections, as well as, errors in the camera parameters and planarity of the calibration target. A solution for the intersection can be obtained to minimize the squared distance between the computed position of the light source and each of the estimated light direction vectors [14]. This can be posed in matrix form as $\mathbf{L} = \mathbf{A}^{-1}\mathbf{b}$ where the matrix $\mathbf{A}$ and vector $\mathbf{b}$ are defined as:

$$\mathbf{A} = \begin{bmatrix} \sum_i (1 - a_i^2) & -\sum_i a_i\, b_i & -\sum_i a_i\, c_i \\ -\sum_i a_i\, b_i & \sum_i (1 - b_i^2) & -\sum_i b_i\, c_i \\ -\sum_i a_i\, c_i & -\sum_i b_i\, c_i & \sum_i (1 - c_i^2) \end{bmatrix}$$

$$\mathbf{b} = \begin{bmatrix} \sum_i \left[(1 - a_i^2) x_i - x_i x_i y_i - a_i\, c_i\, z_i \right] \\ \sum_i \left[-a_i\, b_i\, x_i + (1 - b_i^2) y_i - b_i\, c_i\, z_i \right] \\ \sum_i \left[-a_i\, c_i\, x_i - b_i\, c_i\, y_i + (1 - c_i^2) y z_i \right] \end{bmatrix} \tag{5}$$

The solution for $\mathbf{L}$ provides the optimal estimate for the illumination position in the least-squares sense and can be computed using the Singular Value Decomposition (SVD) of $\mathbf{A}$. We do not consider robust estimation in this study but note that a random sampling approach or a robust error function can be optimized to eliminate outlier directions [16].

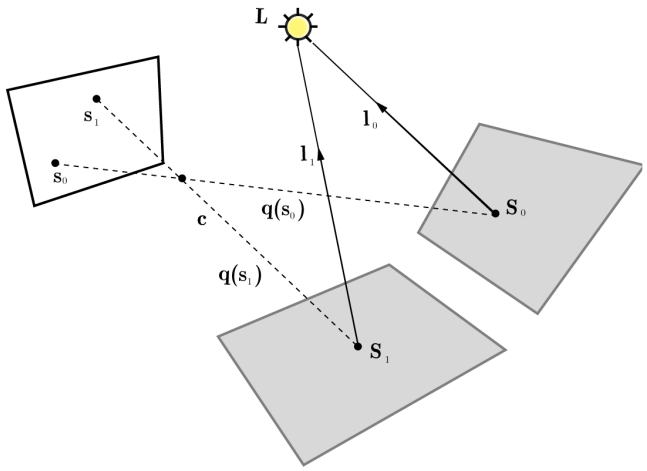

Fig. 3. The overall arrangement of triangulation for the light source position using specular reflections. The different observations of the calibration object provide constraints on the position of the light with respect to the camera coordinate system.

B. Stereo-laparoscope

The above principle can be extended to the stereo-laparoscope case where two observing cameras are used to estimate $\mathbf{L}$. The extrinsic rotation and translation between the two cameras is known from the calibration procedure and therefore for each observation of the target we may obtain two constraint on $\mathbf{L}$, one arising from (4) and the second from the complementary light source direction ray:

$$\mathbf{l}' = \mathbf{q}'(\mathbf{s}') - 2(\mathbf{n} \cdot \mathbf{q}'(\mathbf{s}'))\mathbf{n} \tag{6}$$

where $\mathbf{s}'$ represents the specular point equivalent to $\mathbf{s}$ in the stereo pair image. It should be noted that $\mathbf{s}$ and $\mathbf{s}'$ are not projections of the same 3D point. The reflections are view-dependent at therefore the points $\mathbf{S}$ are not coincident. The collected constraints from all observations can be combined and used to triangulate $\mathbf{L}$ as in the previous section. For scopes with more than one light source, as shown in Fig 1, the specular reflection arising from each light channel needs to be dealt with explicitly. This is not difficult to achieve in practice as the reflections maintain a steady relative orientation in the images.

IV. Experiments and Results

To evaluate the numerical performance of the proposed algorithm against noise and measurement errors, we created a simulation environment where the illumination position and camera parameters are known. Sample calibration objects are randomly generated within the environment inducing specular reflections at variable locations in the image. These synthetic specularities are then used to estimate the illumination position. To generate a synthetic dataset we initially select a random location in the image and compute

the line of sight ray. A calibration object of known orientation is then generated at a random depth in front of the camera and the normal of the object is set to satisfy the camera and light source configuration. All parameters in the environment are known and hence extensive numerical evaluation can be performed.

A. *Simulations for Image Noise*

In our first step of the simulations, we tested against different levels of noise in the measured image coordinates of the specular reflection. To estimate the position of the illumination, we corrupted each specular image point by additive Gaussian noise with 0 mean and standard deviation varying between 0 and 2 pixels. For each noise level, 100 trials were conducted and we measured the mean and standard deviation of the error. To validate the dependence of the algorithm against the number of calibration target orientations required for a solution, we performed each trial for between 0 and 20 views selected at a distance ranging from 50mm to 150mm in front of the camera. The orientation of each target was selected to induce a specularity in the image, after the target's depth was randomly chosen.

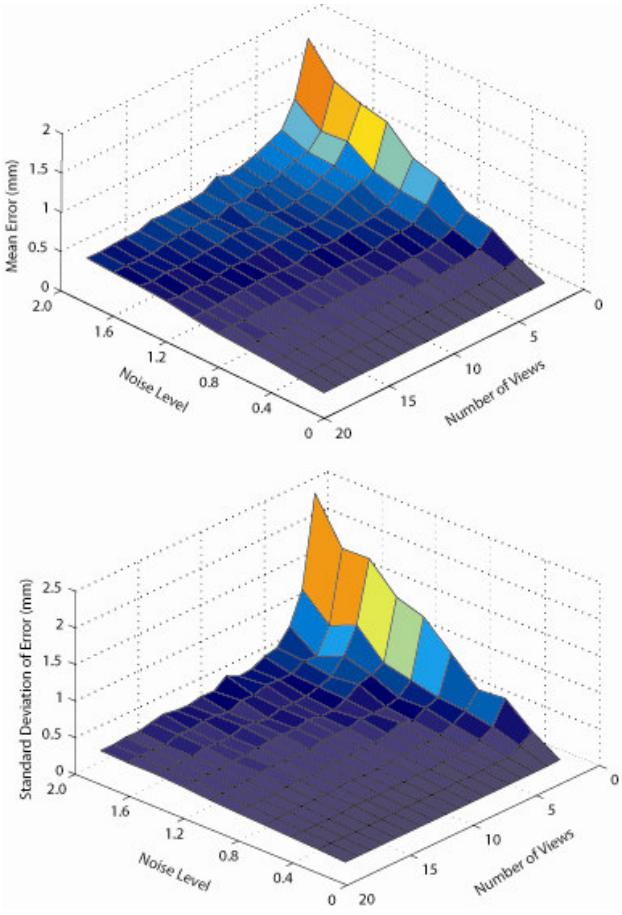

Fig. 4. Surface plots of the mean and standard deviation of the position estimation error with respect to the noise in image measurements and the number of calibration views used.

In Fig 4 we show the resulting error surface plot of the light source position estimate with respect to increasing levels of noise and the number of views used for the estimation. The algorithm can achieve accuracy below 0.5mm despite noisy measurement provided that a sufficient number of observations are made. Performance is more severely affected when the number of views is small. However, in practice it is common and easily manageable to acquire more than 10 observation of the calibration target.

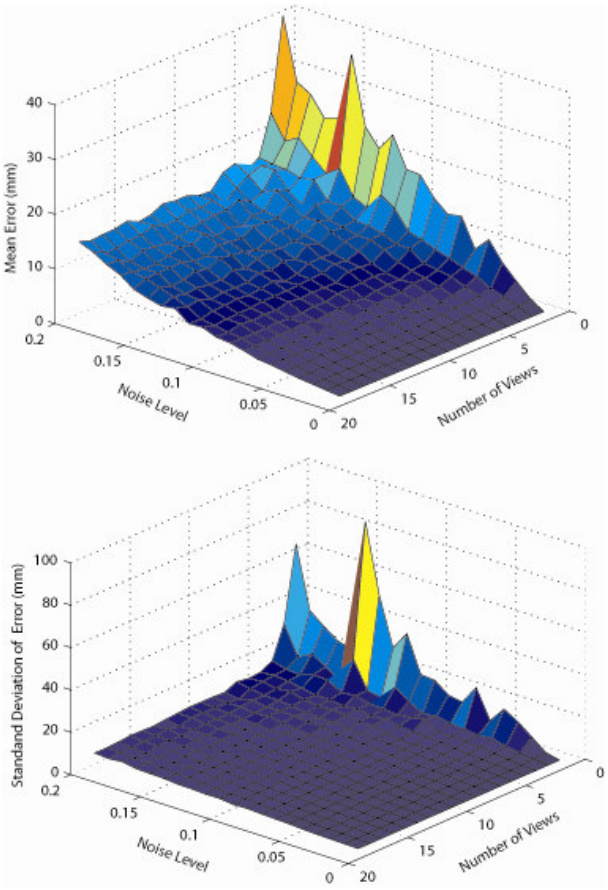

Fig. 5. Surface plots of the mean and standard deviation of the position estimation error with respect to deviation of the normal of the extrinsic object surface.

B. *Simulations for Normal Estimation Errors*

To evaluate performance against errors made for the position and orientation of the calibration object during calibration, we used the simulation framework to corrupt the known plane normal additive Gaussian noise. After setting up the virtual calibration target as described above, the known normal used for estimating $\mathbf{L}$ was induced with noise by from a Gaussian distribution with mean 0 and standard deviation varying between 0 and 0.2 radians. The perturbed normal was then used to estimate the illumination position and we measured the Eucledian error between the known ground truth and the estimate. As before simulations were executed 100 times for each noise and number of views pairing.

In Fig 5 we show the results of our simulations against extrinsic parameter noise. It is evident that the algorithm is sensitive to this measurement error. As with image noise, performance is most severely affected when the number of target observations is small.

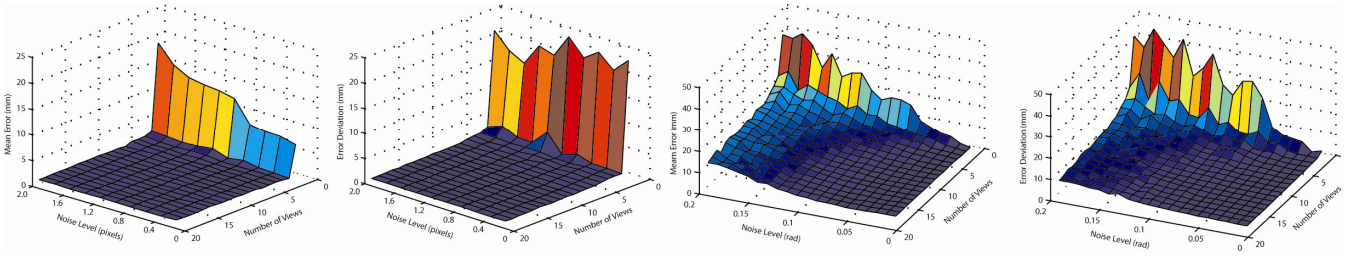

Fig. 6. Surface plots of the error for running simulations against noise in the image space (a-b) and in the extrinsic orientation (c-d) with a virtual stereo-laparoscope. The performance of the algorithm mimics the monocular version, however, errors are considerably smaller as a result of the larger number of constrains obtained by the stereo rig.

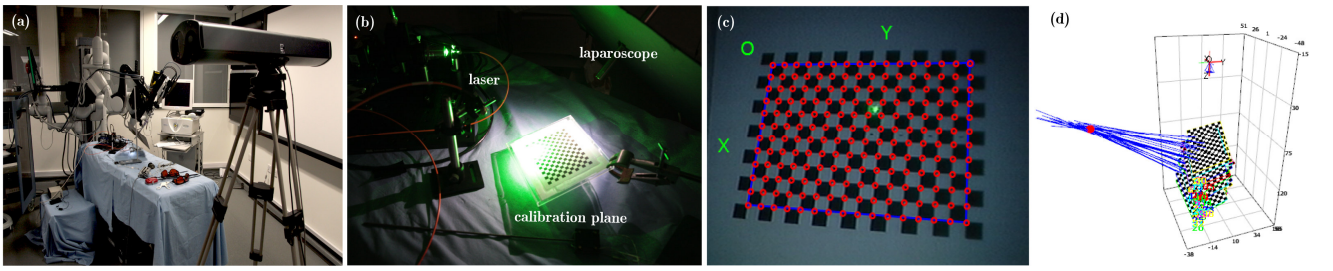

Fig. 7. The experimental setup with a robotic stereo-laparoscope and laser light source (a) illustrates the setup with the optical tracking system used for ground truth validation; (b) close up view of the calibration target, stereo-laparoscope and the laser source; (c) calibration target as observed in the image space with the detected grid points and a clearly visible green speckle from the laser; (d) rendering of the 3D space computed in the camera coordinate system, where the blue rays intersect to localize the illumination source.

C. Simulations for Stereo-laparoscopes

To evaluate the illumination position estimation performance when dealing with a stereo-laparoscope the experiments in the two previous sections were performed with a stereo configuration. To generate consistent synthetic data for both views we used the monocular strategy previously described for the reference camera (left). Data for the stereo pair was then generated by determining the image point that satisfies (4). Noise was then added to each camera's measurements independently and the experimental trials were conducted for different numbers of observations and variable levels of noise. Trials were conducted 100 times at each noise level and number of observations pairing and the mean and standard deviations of the error were recorded.

The surface plots in Fig 6 show that the error for noise in the image coordinates, and in the extrinsic geometry of the calibration plane for the stereo-laparoscope case is significantly lower. The main reason for this is that the number of views used is double and hence quickly stabilizes the estimation's sensitivity to noise by carving away the illumination's position. Another advantage of having the stereo estimation is that a wider set of angles is produced for the triangulation, which inherently improves localization.

D. Experiments with a Point Light Source

To evaluate the proposed algorithm an experiment involving a point laser light source as shown in Fig 7 was performed. Laser light (532 nm, 50 mW, doubled Nd:YAG, Spectra Physics) was focused into a 600 micron step index fused silica optical fibre for delivery to the experiment. The bare output of the fibre formed a 'point' light source with an emitting area of diameter 600 microns and a numerical aperture of 0.22, equivalent to an output cone angle of 0.22 radians. Compared to normal laparoscopes, the laser source reduces the diameter of the illumination and allows more precise evaluation of the position estimation. The stereo-laparoscope of the da Vinci® (Intuitive Surgical® Inc.) surgical system was used to collect images of the calibration target while an optical tracking system (Optotrak, Northern Digital Inc.) was used to obtain ground truth measurements within the setup. Hand-eye calibration between the optical system and the camera was obtained using Tsai's algorithm [17] and a rigid probe was used to measure the position of the laser fibre in the world coordinate system.

We collected calibration images using a specularly reflective planar calibration grid (no explicit tests for planarity were conducted) as shown in Fig. 7. The intrinsic camera parameters were computed using the implementation of [18] in our publicly available software. In a future release, this will include an implementation of the method proposed in this study (http://www.doc.ic.ac.uk/~dvs/calib/main.html). Specular points were detected by thresholding the intensity image and taking the centre of mass for specular pixels. While not very robust, this approach performed well in practice as the illumination intensity can be controlled at the Xenon source to attenuate speculaties. The rays defined by the calibration grid's orientation and the specular surface point were then used to estimate the laser fibre's position as shown in the 3D rendition in Fig 7. The error of the estimate compared to the ground truth position determined using the optical probe was measured at 2.12mm. It is important to note that this error includes the error of the optical tracking system, which was estimated to be in the range of 1.5mm.

TABLE I
RESULTS FOR EXPERIMENTS ON REAL DATA

Calibration Plane Dimensions (size)	Calibration Views	Calibration Reprojection Error (pixels)	Illumination Estimation Views	Illumination Position Estimate	Normal Testing Views	Normal Estimation Error (deg)
11x15 (5.5mm)	15	[0.134, 0.126]	10	[5.58,-4.23,0.59]	5	3.13±1.52
11x15 (5.5mm)	15	[0.109, 0.099]	10	[5.48,4.76,0.43]	5	2.81±.2.01
11x15 (5.5mm)	15	[0.119, 0.113]	10	[5.13,4.18,0.45]	5	2.33±.1.78
11x15 (3.4mm)	10	[0.092, 0.096]	7	[4.37,-3.95,0.13]	3	1.97±1.25
11x15 (3.4mm)	10	[0.105, 0.107]	7	[3.98,3.96,0.73]	3	2.19±2.21
11x15 (3.4mm)	10	[0.112, 0.115]	7	[4.12,3.63,-0.21]	3	2.79±2.10

E. Experiments with a Stereo-laparoscope

In order to illustrate the performance of the calibration algorithm in a practical scenario, we provide qualitative analysis of estimating the illumination sources' position for the da Vinci® system's stereo-laparoscope. We collect calibration images as previously described and for each image detect the specular highlights caused by the incoherent fibre bundle illumination sources at the scope's tip. The results of applying the monocular and stereoscopic version of the proposed method are shown in Table 1. For each dataset we used variable numbers of images to obtain the light source position and qualitatively we see that the estimated 3D points are consistent. Furthermore, we should note that the diameter of each light source at the exit point of the scope is approximately 2mm. Therefore the estimation is likely to be subject to some error as the position can fall anywhere within this region.

In addition to measuring the estimated position, we tested estimating the normal of the calibration plane at the specular point. This was performed for images not used in the calibration dataset itself and hence not influenced by the estimation. From the results in Table 1 it is evident that the proposed method can compute the normal of the surface at specular points with a good degree of accuracy.

V. CONCLUSION

In this paper, we have developed a practical strategy for determining the light source position with respect to the camera for laparoscope and stereo-laparoscope devices. Our technique uses constraints obtained from specular reflections on a traditional calibration plane used in determining the optical parameters of the cameras. Experiments with simulations and a practical setup have illustrated the potential of the proposed method. This is an important step towards more accurate techniques for optically based 3D reconstruction and soft-tissue morphology estimation in vivo. In future work, we will demonstrate the effect of illumination position on surface shape estimation techniques and we will determine the illumination source's irradiance function with respect to the distance of the calibration object.

REFERENCES

[1] R. H. Taylor and D. Stoianovici, "Medical Robotics in Computer-Integrated Surgery," *IEEE Trans on Robotics and Automation,* vol. 19, pp. 765-781, 2003

[2] H. Delingette, X. Pennec, L. Soler, J. Marescaux, and N. Ayache, "Computational Models for Image-Guided Robot-Assisted and Simulated Medical Interventions," *Proceedings of the IEEE,* vol. 94, pp. 1678-1688, 2006

[3] D. Stoyanov, G. Mylonas, A. J. Chung, M. Lerotic and G.-Z. Yang, " Intra-operative Visualisations: Perceptual Fidelity and Human Factors," *IEEE/OSA Journal of Display Technologies*, vol. 4(4), pp. 491-501, 2008

[4] T. Okatani and K. Deguchi, "Shape Reconstruction from an Endoscope Image by Shape from Shading Technique for a Point Light Source at the Projection Centre," *Computer Vision and Image Understanding,* vol. 66, pp. 119-131, 1997

[5] H. U. Rashid and P. Burger, "Differential algorithm for the determination of shape from shading using a point light source" *Image and Vision Computing,* vol. 10, pp. 119 - 127 1992

[6] B. Craine, C. E.R., C. O'Toole, and Q. Ji, "Digital imaging colposcopy Corrected area measurements using Shape-from-Shading" *IEEE Trans on Medical Imaging*, vol. 17(6), pp. 1003–1010, 1998

[7] A. Tankus, Nir Sochen and Yehezkel Yeshurun, "A New Perspective on Shape from Shading", in *International Conference on Computer Vision*, vol. 2, pp. 862-869, 2003

[8] M. Nicolaou, A. James, B. P. L. Lo, A. Darzi, G.-Z. Yang, "Invisible Shadow for Navigation and Planning in Minimal Invasive Surgery" in *International Conference on Medical Image Computing and Computer Assisted Intervention*, vol. 2, pp. 25-32, 2005

[9] D. Stoyanov, A. Darzi and G.-Z. Yang, "Dense 3D depth recovery for soft tissue deformation during robotically assisted laparoscopic surgery," in *International Conference on Medical Image Computing and Computer Assisted Intervention*, vol. 2, pp. 41-48, 2004

[10] W. W. Lau, N. A. Ramey, J. Corso, N. V. Thakor, and G. D. Hager, "Stereo-Based Endoscopic Tracking of Cardiac Surface Deformation," in *International Conference on Medical Image Computing and Computer Assisted Intervention*, vol. 1, pp. 494-501, 2004

[11] R. Richa, P. Poignet, C. Liu, " Efficient 3D Tracking for Motion Compensation in Beating Heart Surgery," in *International Conference on Medical Image Computing and Computer Assisted Intervention*, vol. 2, pp. 684-691, 2008

[12] D. Stoyanov and G. Z. Yang, "Removing Specular Reflection Components for Robotic Assisted Laparoscopic Surgery," in *IEEE International Conference on Image Processing*, pp. 350-359, 2005

[13] M. Gröger, T. Ortmaier, W. Sepp and G. Hirzinger, "Reconstruction of image structure in presence of specular reflections," in *Pattern Recognition, 23rd DAGM Symposium*, pp. 53-60, 2001

[14] J. E. Solem and A. Hayden, "Estimating Surface Shape and Extending Known Structure Using Specular Reflections", in *International Conference on Pattern Recognition*, pp. 173-176, 2004

[15] A. Criminisi, S. B. Kang, R. Swaminathan, R. Szeliski, P. Anandan, "Extracting layers and analyzing their specular properties using epipolar-plane-image analysis," *Computer Vision and Image Understanding*, vol. 1, pp. 51-85, 2005

[16] R. Hartley and A. Zisserman, *Multiple View Geometry in Computer Vision*, Cambridge Press, 2001

[17] Z. Zhang, "A Flexible New Technique for Camera Calibration," *IEEE Transactions on Pattern Analysis and Machine Intelligence,* vol. 22, pp. 1330-1334, 2000

[18] R. Y. Tsai and R. K. Lenz, "Real Time Versatile Robotics Hand/Eye Calibration using 3D Machine Vision*" IEEE International Conference on Robotics and Automatio*, vol. 1, pp. 554 – 556, 1988